Cell Stem Cell
Resource

Modeling Disease in Human ESCs Using an Efficient BAC-Based Homologous Recombination System

Hoseok Song,[1,2] Sun-Ku Chung,[1,2] and Yang Xu[1,*]
[1]Section of Molecular Biology, Division of Biological Sciences, University of California, San Diego, 9500 Gilman Drive, La Jolla, CA 92093-0322, USA
[2]These authors contributed equally to this work
*Correspondence: yangxu@ucsd.edu
DOI 10.1016/j.stem.2009.11.016

SUMMARY

Although mouse models have been valuable for studying human disease, the cellular and physiological differences between mouse and human have made it increasingly important to develop more relevant human disease models for mechanistic studies and drug discovery. Human embryonic stem cells (hESCs), which can undergo unlimited self-renewal and retain the potential to differentiate into all cell types, present a possible solution. To improve the efficiency of genetic manipulation of hESCs, we have developed bacterial artificial chromosome (BAC) based approach that enables high efficiency homologous recombination. By sequentially disrupting both alleles of ATM or p53 with BAC targeting vectors, we have established ATM$^{-/-}$ and p53$^{-/-}$ hESCs as models for two major human genetic instability syndromes and used the generated cells to reveal the importance of p53 in maintaining genome stability of hESCs. Our findings suggest that it will be feasible to develop genetically modified hESCs as relevant human disease models.

INTRODUCTION

Mouse knockin and knockout technologies have allowed the generation of mouse models for human genetic diseases, studies of which have provided considerable mechanistic insight on the pathogenesis of human diseases. However, many apparent cellular and physiological differences between mouse and human make it difficult for mouse models to recapitulate all mechanisms of pathogenesis in human patients and lead to the common phenomenon that therapeutic interventions work well in mouse models but poorly in human patients. Therefore, there is an increasing demand for more relevant human disease models. Human embryonic stem cells (hESCs) are capable of unlimited self-renewal and retain the pluripotency to differentiate into all cell types of the human body in vitro and in vivo. Therefore, the disease-specific hESCs could provide the much-needed human disease models that are complementary to mouse models for mechanistic studies and drug discovery.

Despite the great potential of hESCs in modeling human genetic diseases, this area of research has been largely stalled due to the technical difficulty in genetically modifying hESCs. While a number of reported studies have used standard plasmid vectors to target endogenous genes through homologous recombination in hESCs (Urbach et al., 2004; Costa et al., 2007; Davis et al., 2008; Xue et al., 2009; Irion et al., 2007; Ruby and Zheng, 2009; Zwaka and Thomson, 2003), the targeting efficiency is usually low. In addition, there have been few successes of homozygous disruption of a gene in hESCs. To address this bottleneck, we have adapted and optimized the bacterial artificial chromosome (BAC)-based targeting approach that routinely enables high efficiency homologous recombination in hESCs. As a proof of principles, we have employed this BAC-based targeting approach to generate ATM$^{-/-}$ and p53$^{-/-}$ hESCs that provide the disease models for two major human cancer and genetic instability syndromes.

ATM is a protein kinase mutated in the human genetic instability syndrome Ataxia-telangiectasia (Lara-Tejero and Galán, 2000), which is characterized by multisystemic defects, including growth retardation, neuronal degeneration, telangiectasia, male and female germ cell defects, immunodeficiency, greatly increased cancer risk and hypersensitivity to ionizing radiation (Shiloh, 1995). A-T cells undergo reduced proliferation and premature senescence and are radiosensitive with increased genetic instability, such as chromosomal translocation (Shiloh and Kastan, 2001). To investigate the physiological roles of ATM in DNA-damage responses and mammalian development, ATM-deficient mice have been established that recapitulate many A-T systemic and cellular defects, including radiosensitivity, immunodeficiency, high incidence of cancer, and abolished germ cell development (Barlow et al., 1996; Elson et al., 1996; Xu et al., 1996; Xu and Baltimore, 1996). However, several A-T-related defects, such as apparent neuronal degeneration and accelerated shortening of telomeres, are not evident in ATM-deficient mice.

p53 is the most commonly mutated tumor suppressor in human cancers and plays critical roles in cell-cycle arrest, cellular differentiation and apoptosis, and DNA repair (Mills, 2005). All these functions of p53 are important to maintain genetic stability by preventing the genome from accumulating mutations and passaging these mutations to the daughter cells.

p53 is a transcription factor with a sequence-specific DNA-binding domain in the central region and a transcriptional activation domain at the N-terminus (Ko and Prives, 1996). Three additional domains, including a nuclear localization signal, a tetramerization domain, and an extreme C-terminal regulatory domain, are present in the C terminus of p53 (Ko and Prives, 1996). For over a decade, $p53^{-/-}$ mice have been used extensively in cancer research. However, $p53^{-/-}$ mice fail to recapitulate the tumorigenesis in human patients. In this context, while $p53^{-/-}$ mice uniformly died of thymic lymphomas and sarcomas (Donehower et al., 1992; Jacks et al., 1994), human cancer patients mostly develop carcinomas. In addition, while p53 is required for G_2/M checkpoint in human cells, it is dispensable for G_2/M checkpoint in mouse cells (Sancar et al., 2004; Song et al., 2007). Therefore, the $ATM^{-/-}$ and $p53^{-/-}$ hESCs provide unique opportunity to further study the roles of these critical tumor suppressors in maintaining genetic stability in hESCs and tumor suppression in humans.

RESULTS

Targeted Disruption of the *ATM* Gene in hESCs with BAC-Based Vectors

Based on our experience with genetic manipulation in mouse ESCs, the capability of a single hESC to undergo self-renewal and expand into an entire colony without incurring differentiation and genetic instability is a prerequisite for the success of genetic manipulation. After experimenting with the existing hESC lines, we found that the HUES lines, which can be passaged as single cells, are suitable for this purpose (Cowan et al., 2004). To disrupt the *ATM* gene in hESCs, we initially constructed a conventional targeting vector with limited sizes (9 Kb and 2 kb) of homologous arms. The very low targeting efficiency (<0.5%) makes it impractical to sequentially target both alleles of ATM in hESCs (data not shown). To increase the frequency of homologous recombination in hESCs, we employed the recombineering technology to develop bacterial artificial chromosome (BAC)-based targeting vectors that harbor much larger size of homologous arms (Copeland et al., 2001). To ensure the disruption of the expression of the targeted genes, a splicing acceptor was present between the CAG promoter and neomycin resistance gene (Neo) to disrupt the normal splicing of the targeted gene locus, leading to a fusion of upstream exon and Neo (Figure 1B). In addition, the CAG-Neo selection cassette dramatically suppresses the expression of the targeted allele. To allow the screening of the homologous recombinants by Southern blotting, the size of one homologous arm of the BAC-targeting vector was shortened with recombineering.

The linearized BAC-targeting vector was transfected into hESCs and selected with G418 for 2 weeks. The surviving colonies were individually picked and expanded, and genomic DNA was screened for homologous recombination. We usually obtained 10–50 colonies after electroporating 100 μg linearized BAC vectors into 20 million HUES9 cells. Since standard PCR assay cannot be used to identify the homologous recombinants due to the large sizes of the flanking homologous arms, we designed a ligation-mediated PCR that can be universally adapted to screen homologous recombinants involving BAC-based targeting vectors (Figure 1C). In this context, the genomic DNA of individual clones was digested with NcoI, whose restriction site lies in the selection marker and the genomic DNA outside the shorter homology arms, and religated (Figure 1C). When amplified by nested PCR reactions with primers 3 and 4 followed by primers 1 and 2, only the DNA from the homologous recombinants would give rise to a 332 bp PCR product (Figure 1D). Three of the 14 clones obtained from one round of electroporation were positive for homologous recombination event, indicating a greatly increased targeting frequency of 21%. The $ATM^{+/-}$ hESCs were confirmed to have normal karyotypes (Figure S1A available online).

To target the remaining WT allele in $ATM^{+/-}$ hESCs, we used the same BAC vector, except changing the selection cassette to CAG-Neo-IRES-Puro so that the transfectants are resistant to puromycin (Figure 1C). Neo was retained in the selection cassette, as it is required to confer kanamycin resistance to the bacteria that have undergone recombineering. The homologous recombinants were also screened by ligation-mediated PCR with primers 4 and 6 followed with primers 1 and 5; only homologous recombinant will give rise to a 531 bp PCR product (Figures 1C and 1D). Ten of the 37 clones obtained from one round of electroporation were positive for the homologous recombination event, indicating a targeting efficiency of 27%. In two of the ten positive clones, the WT allele was targeted to generate homozygous mutant hESCs. The homozygous mutant hESCs were confirmed by Southern blotting (Figure 1E). To further ensure that there is no aberrant rearrangement between the large homologous arm of BAC vector and the endogenous locus, genomic DNA derived from $ATM^{-/-}$ hESCs were analyzed by Southern blotting with a mixture of probes spanning throughout the long arm of the BAC vector, indicating that there was no random integration or aberrant rearrangement (Figure S1B). Consistent with the lack of random integration in $ATM^{-/-}$ hESCs, we detected only two copies of the ATM loci in $ATM^{-/-}$ hESCs using a Taqman quantitative PCR assay (Figure S1C). In further support of the lack of random integration of the targeting vector in $ATM^{-/-}$ hESCs, SNP-CGH array analysis showed no apparent alteration at the SNPs spanning the *ATM* loci in $ATM^{-/-}$ hESCs (Figure S1D). However, as a common issue for all genetic manipulation approaches that require transfection of exogenous DNA into hESCs, we cannot rule out the possibility of the random integration of small DNA pieces of the targeting vector into the genome. This issue could only be addressed by whole genome sequencing of the targeted hESCs.

To confirm that the expression of ATM is disrupted in $ATM^{-/-}$ hESCs, the expression of ATM protein in the homozygous mutant hESCs was analyzed, indicating that these mutant hESCs are indeed $ATM^{-/-}$ (Figure 1F).

Targeted Disruption of the *p53* Gene in hESCs

To test whether the BAC-based approach can be employed to efficiently target other locus, recombineering technology was also used to develop BAC-based targeting vectors to disrupt the *p53* gene in hESCs (Figure 2B). To generate $p53^{+/-}$ hESCs, WT hESCs were transfected with a BAC targeting vector that was designed to delete exons 2–6 of human *p53* (Figure 2B). The targeting frequency was two in about 60 clones obtained from two rounds of electroporation, and the homologous

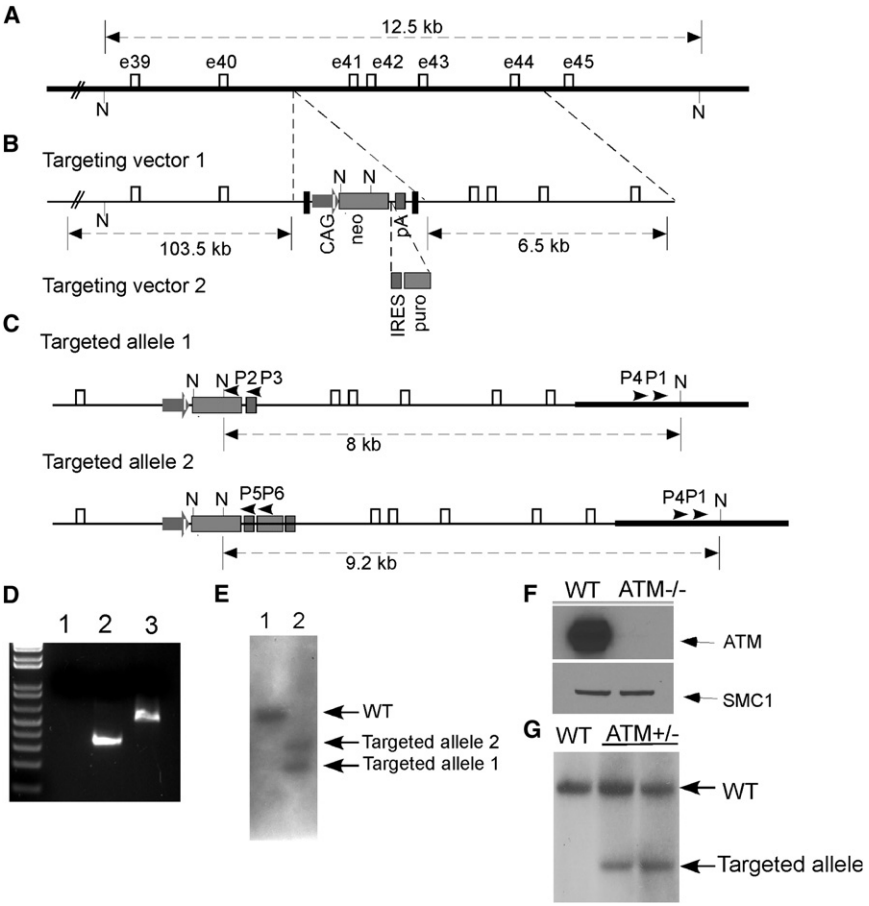

Figure 1. The Generation of ATM$^{-/-}$ hESCs

(A) The endogenous ATM locus in humans. The exons are indicated by open boxes. The initiation ATG is located 85 Kb upstream from the exon 40. The size of the NcoI (N) restriction fragment is indicated.

(B) BAC-based targeting vectors. In targeting vector 1, the selection cassette CAG-Neo was inserted into intron 40 by recombineering. In targeting vector 2 used to target the WT allele in ATM$^{+/-}$ hESCs, the selection marker cassette CAG-Neo-IRES-Puro was inserted into the same site of intron 40 by recombineering. The sizes of the homologous arms are indicated.

(C) The configuration of the both targeted ATM alleles in ATM$^{-/-}$ hESCs. The primers (P1–P6) used to detect homologous recombination by ligation-mediated PCR are indicated by arrowheads. The sizes of the NcoI (N) restriction fragments of both targeted alleles are indicated.

(D) Representative data of ligation-mediated PCR to detect the targeting of both ATM alleles via homologous recombination. Genomic DNA was digested with NcoI, religated, and amplified by nested PCR with primers P1–P6. Lane 1, WT hESCs; Lane 2, hESCs in which the ATM allele was targeted by vector 1; Lane 3, hESCs in which the ATM allele was targeted by vector 2.

(E) Southern blotting analysis of WT (lane 1) and ATM$^{-/-}$ (lane 2) HUES9 hESCs. Genomic DNA was digested with NcoI and hybridized with a cDNA probe spanning exons 43–45. The restriction fragments derived from WT and two targeted alleles are indicated.

(F) The ATM protein is undetectable in ATM$^{-/-}$ hESCs by western blotting analysis. ATM and the loading control SMC1 are indicated.

(G) Southern blotting analysis of ATM$^{+/-}$ H9 hESCs as described in (E). Data from two independent H9 ATM$^{+/-}$ clones are shown. See also Figure S1.

recombinants were confirmed by Southern blotting (Figures 2B, 2D, and 2F). The relatively low targeting efficiency is likely due to the relatively short homologous arms of the targeting vector. After confirming that the p53$^{+/-}$ hESCs have normal a karyotype (Figure S2A), the p53$^{+/-}$ hESCs were transfected with a BAC-targeting vector that harbors longer homologous arms and CAG-Neo-IRES-Puro selection cassette (Figure 2C). The homologous recombination between the targeting vector and the WT allele in p53$^{+/-}$ hESCs were screened by PCR with primers P1–P3 that amplify the targeted allele (P1 + P2) and the WT allele (P1 + P3) in p53$^{+/-}$ hESCs (Figures 2D and 2E). If homologous recombination occurs between the WT allele and the targeting vector, there should be no amplification of the WT allele by primers P1 + P3. Seven of the 32 clones obtained from one round of electroporation had undergone homologous recombination between the WT allele and the targeting vector, giving a targeting efficiency of 22% (Figure 2E). The homozygous p53 mutant hESCs were confirmed by Southern blotting (Figure 2F). To confirm that there was no aberrant rearrangement between the longer arm of the BAC vector and the endogenous locus in the targeted hESCs, the genomic DNA from heterozygous and homozygous mutant hESCs were also analyzed by Southern blotting with various enzymatic digestion and hybridization to a mixture of probes within the targeting vector, indicating no random integration of the targeting vector or aberrant rearrangement (Figure S2B). The homozygous mutant hESC clones have no detectable p53 protein even after DNA damage that greatly increases p53 protein levels in WT hESCs, confirming that these hESCs are indeed p53$^{-/-}$ (Figure 2G).

BAC-Based Targeting Strategy Works Well in Other hESC Lines and Genetic Loci

To test whether the BAC-based targeting strategy can be applied to other hESC lines, we determined the targeting efficiency of the BAC vector in disrupting the ATM gene in the traditional hESC line H9. H9 cells were not suitable for clonal selection because they must be passaged as clumps of cells and undergo massive apoptosis when dissociated as single cells. This problem was mitigated by a recent finding that a ROCK inhibitor Y-27632 greatly increases cloning efficiency of hESCs without affecting their pluripotency and genomic stability (Watanabe et al., 2007). By treating the H9 hESCs with Y-27632 for 2 hours before electroporation and for 24 hr after

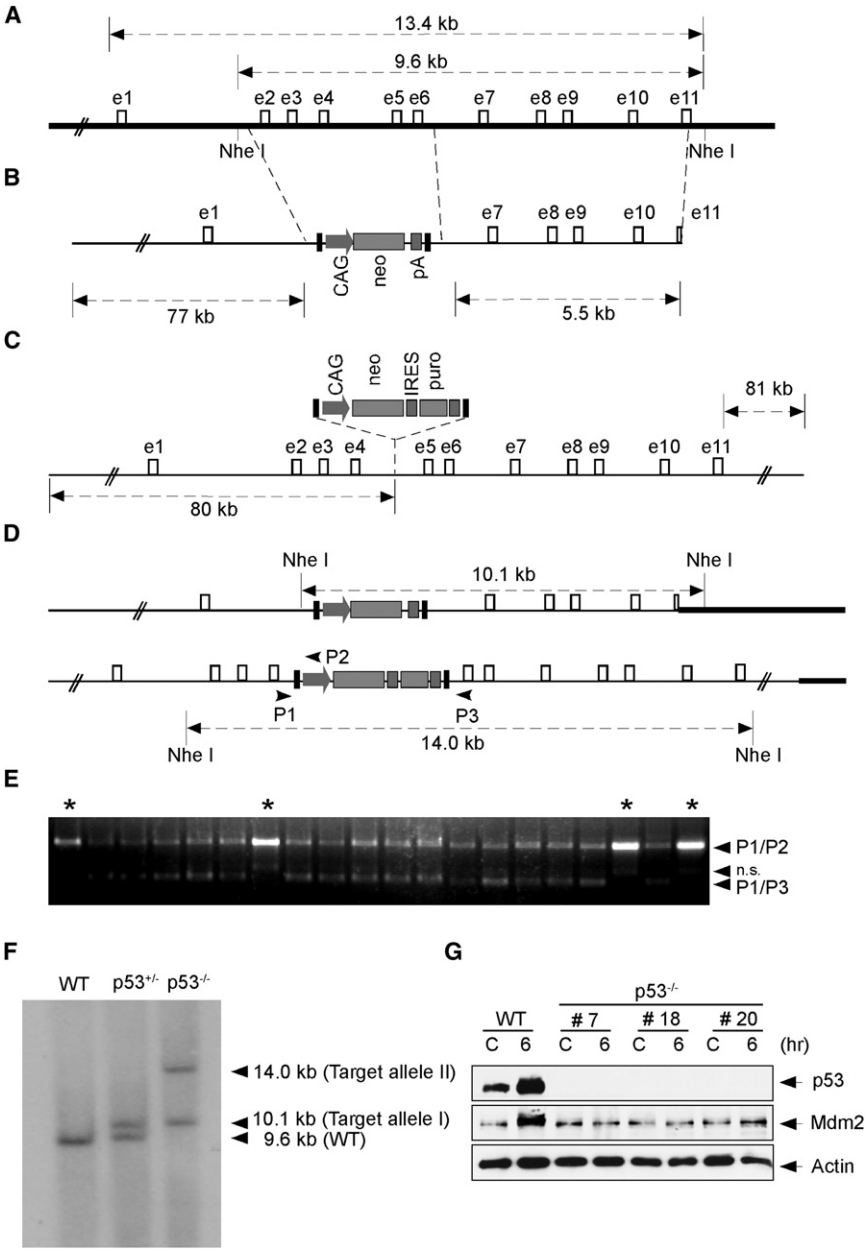

Figure 2. The Generation of p53$^{-/-}$ hESCs

(A) The endogenous p53 locus in hESCs. The size of NheI fragment is indicated. Open boxes represent exons. The initiating ATG is in exon 2.

(B) BAC-based targeting vector to delete exons 2–6 of human p53 gene. The sizes of flanking homologous arms are indicated.

(C) BAC-based vector to target the WT p53 allele in p53$^{+/-}$ hESCs. The selection marker cassette CAG-Neo-IRES-Puro was inserted into the intron 4. The sizes of the flanking homologous arms (80 kb and 81 kb) are indicated.

(D) The configuration of both targeted p53 alleles in p53$^{-/-}$ hESCs. The forward (P1) and two reverse (P2 and P3) primers used for PCR screening of homozygous targeting are indicated by arrowheads.

(E) Representative PCR data to identify p53$^{-/-}$ hESCs. Genomic DNA was amplified by PCR with primers (P1 + P2 + P3). The targeting of the WT allele in p53$^{+/-}$ hESCs leads to the loss of any amplification by P1 + P3 due to the large size of selection marker. The positive clones are marked by asterisks. N.S. means nonspecific PCR product.

(F) Genomic DNA of WT, p53$^{+/-}$, and p53$^{-/-}$ was digested with NheI and hybridized with a cDNA probe spanning exons 5–10. The restriction fragments derived from WT and two targeted alleles are indicated.

(G) The p53 protein was undetectable in p53$^{-/-}$ hESCs before and after DNA damage induced by doxorubicin (0.2 μM). p53, Mdm2, and actin are indicated. See also Figure S2.

electroporation of the ATM targeting BAC vector, we obtained over 100 colonies from two rounds of electroporation. Sixteen of the 76 clones screened were positive for homologous recombination at the *ATM* locus, indicating a targeting efficiency of 21% (Figure 1G). Therefore, the BAC targeting vector can achieve high efficiency of homologous recombination independent of the genetic background of hESCs.

Both ATM and p53 are important in maintaining genomic stability and regulating cell survival. To rule out the possibility that the high targeting efficiency is due to the selection for improved survival of hESCs impaired in ATM or p53, we developed a BAC targeting vector to disrupt the X-linked Hypoxanthine-Guanine Phosphoribosyl Transferase (*HPRT*) gene (Figures 3A and 3B). To facilitate the analysis, the BAC *HPRT* targeting vector was electroporated into HUES3 and HUES8 hESCs, both of which are male cells and, thus, have only one X chromosome. One of the three puromycin-resistant HUES3 clones and one of the six puromycin-resistant HUES8 clones screened had their *HRPT* gene disrupted, indicating a high efficiency of gene targeting with the *HPRT* BAC vector (Figure 3C). As expected, HPRT knockout hESCs are hypersentitive to HAT (Figure 3D). In summary, our findings indicate that the efficient BAC targeting strategy is applicable to various hESC lines and gene loci.

ATM$^{-/-}$ hESCs and Fibroblasts Recapitulate the Cellular Defects of A-T Patients

ATM deficiency leads to radiosensitivity and defective cell-cycle checkpoints in A-T patients (Xu, 2006). Consistent with this notion, ATM$^{-/-}$ hESCs are hypersensitive to γ-irradiation and defective in G_2/M checkpoint after IR (Figures 4A and 4B). In addition, ATM-dependent phosphorylation of its targets, including SMC1, CHK2, p53, and H2AX, is abolished after IR (Figure 4C). Despite these apparent defects in DNA repair and cell-cycle checkpoints, ATM$^{-/-}$ hESCs exhibit normal karyotypes (Figure S1E). In addition, SNP-CGH array analysis of ATM$^{-/-}$ hESCs indicated no apparent genomic alteration

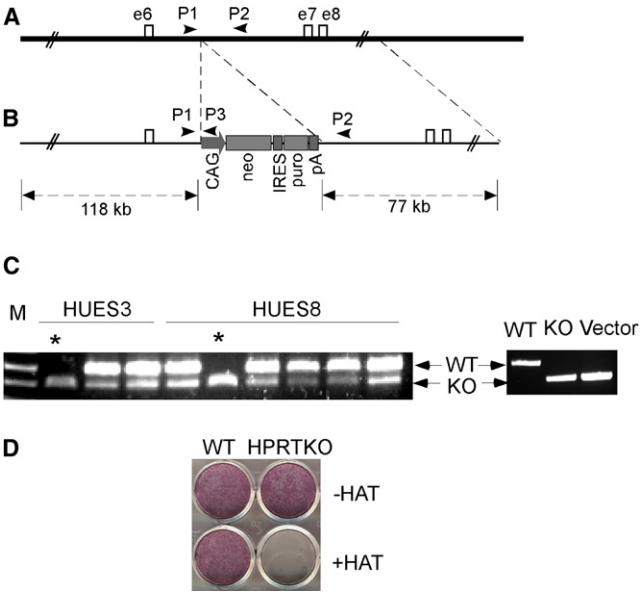

Figure 3. Targeting HPRT Locus with a BAC Vector

(A) The endogenous locus of HPRT locus. Exons are represented by open boxes.

(B) BAC targeting vector. The sizes of the homologous arms are shown. The primers P1–P3 used for screening are indicated.

(C) Disruption of the HPRT gene in the male HUES3 and HUES8 hESCs that have only one X chromosome. After the transfection of BAC vector into HUES3 and -8, both of which are male, the transfectants were selected with puromycin without any 6-TG counter selection to reveal the frequency of homologous recombination. The homologous recombination event was detected by PCR with primers P1–P3, giving rise to a 495 bp product from the WT allele (P1 + P2) and a 393 bp product from the targeting vector or targeted allele (P1 + P3). Homologous recombination between the targeting vector and the only HPRT gene in hESCs leads to the loss of the WT PCR product (lanes marked with asterisks). KO, HPRT knockout hESCs; vector, BAC targeting vector.

(D) HPRT knockout hESCs are hypersensitive to Hypoxanthine-Aminopterin-Thymidine (HAT). WT and HPRT knockout hESCs were plated onto 12-well plate at a density of 10^4 cells/well, and 1 day later, mock-treated or selected with medium containing 1× HAT (Sigma). Five days later, hESCs were visualized by staining for alkaline phosphatase.

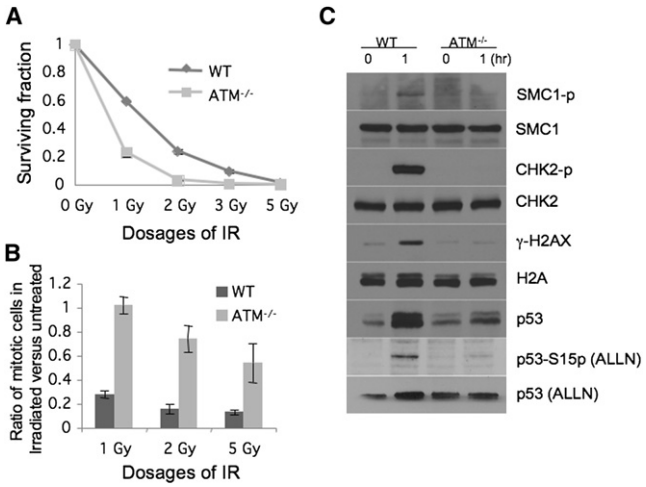

Figure 4. ATM-Dependent Cellular Responses to DNA DSB Damage Are Abolished in ATM$^{-/-}$ hESCs

(A) ATM$^{-/-}$ hESCs are hypersensitive to IR.

(B) ATM$^{-/-}$ hESCs are impaired in G_2/M checkpoint after IR. Mean values from three independent experiments are shown with standard derivation.

(C) ATM-dependent phosphorylation of SMC1 at Ser957, CHK2 at Thr68, p53 at Ser15, and H2AX at Ser139 (γ-H2AX) is abolished in ATM$^{-/-}$ hESCs after IR. p53 stabilization after IR is impaired in ATM$^{-/-}$ hESCs. Therefore, p53 protein was stabilized with proteosome inhibitor ALLN. The phosphorylated and total protein are indicated. Consistent data were obtained from two independent ATM$^{-/-}$ hESC clones.

(Figure S1D). Therefore, unlike those in somatic cells, ATM-independent pathways are sufficient to maintain genetic stability in hESCs.

The power of hESCs in modeling human diseases is that hESCs can be reproducibly differentiated into various primary cell types, such as fibroblasts, for further study (Johnson et al., 2008). By differentiating hESCs into fibroblasts using an EB-mediated protocol (Figure 5A), we further characterized the ATM-dependent responses to DNA damage in human fibroblasts. Irradiation-induced foci formation (IRIF) of DNA repair proteins, including phosphorylated ATM and H2AX (γ-H2AX), is important for initiating DNA DSB damage responses (Xu, 2006). IRIF of phosphorylated ATM and H2AX is abolished in ATM$^{-/-}$ fibroblasts (Figure 5B). Therefore, hESC-derived fibroblasts provide another primary cell type that can be used to study the mechanism of pathogenesis in A-T. In summary, these data demonstrate that ATM$^{-/-}$ hESCs and primary cells derived from them recapitulate the cellular defects observed in A-T patients.

In Vivo Differentiation of ATM$^{-/-}$ hESCs

To confirm the hESC status of ATM$^{-/-}$ hESCs, the ATM$^{-/-}$ hESCs were analyzed for the expression of a panel of hESC-specific surface markers, including TRA-1-60, SSEA3, and SSEA4. This analysis indicates that ATM$^{-/-}$ hESCs express hESC-specific markers indistinguishably from the parental hESCs (Figure S3A). When implanted into the severe combined immunodeficient (SCID) mice, undifferentiated hESCs can form well-differentiated teratomas-like mass that contains the cells differentiated from each of the three germ layers (Thomson et al., 1998). This provides an in vivo system to examine the pluripotency of ATM$^{-/-}$ hESCs and the roles of ATM in human development. ATM$^{-/-}$ hESC clones were injected subcutaneously into right side of the SCID mice. The same number of parental WT hESCs was injected into the left side of the same mice as an internal control. Like parental WT hESCs, ATM$^{-/-}$ hESCs can give rise to teratomas-like mass that contain the cells differentiated from each of the three embryonic germ layers, indicating that the ATM$^{-/-}$ hESCs are pluripotent (Figure 6A). However, the size of the tumors derived from ATM$^{-/-}$ hESCs is about 30% of that derived from WT hESCs, indicating a growth retardation phenotype similarly to that observed in A-T patients (Figure 6B). Since ATM$^{-/-}$ hESCs proliferate similarly to WT parental hESCs, this growth retardation phenotype is not due to any proliferative defects of ATM$^{-/-}$ hESCs (Figure S3B).

A-T patients develop ataxia at a very young age, generally thought as a result of Purkinje cell degeneration (Shiloh, 2003). However, no apparent Purkinje cell degeneration can be detected in ATM$^{-/-}$ mice. To preliminarily test the role of ATM in human neural development, we compared the neural

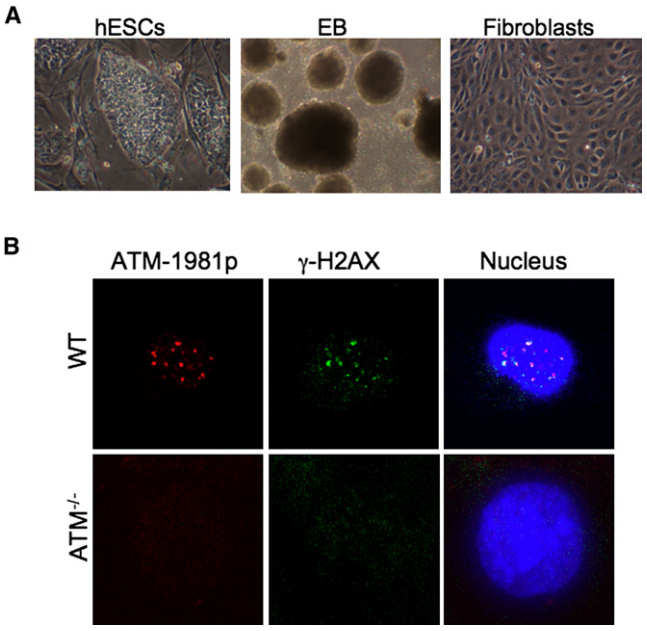

Figure 5. Human Fibroblasts Derived from ATM$^{-/-}$ hESCs Lack Irradiation-Induced Foci of γ-H2AX after IR

(A) EB-mediated differentiation of hESCs into fibroblasts. Representative images of hESCs, day 7 embryoid bodies (EBs), and fibroblasts derived from EBs.

(B) Irradiation-induced foci (IRIF) of phosphorylated ATM and γ-H2AX is abolished in human fibroblasts derived ATM$^{-/-}$ hESCs after IR. The nucleus was counterstained with DAPI.

development in the teratomas derived from WT and ATM$^{-/-}$ hESCs. Similar to those derived from WT hESCs, neural rosettes that represent neural stem cells could be readily identified in the teratomas derived from ATM$^{-/-}$ hESCs (Figure 6A). In addition, the mRNA expression of two neural markers, Neural cell adhesion molecule 1 (NCAM1) and Phosphate-activated glutaminase (GLS2), is similar in the teratomas derived from WT and ATM$^{-/-}$ hESCs, suggesting that ATM is not required for the early human neural development (Figure 6C). While the expression of the Purkinje cell marker glutamate receptor delta-2 (GRID2) was reduced in the teratomas derived from ATM$^{-/-}$ hESCs when compared with that in teratomas derived from WT hESCs, the expression of two other potential Purkinje cell-specific markers (CALB1 and ITPR1) was similar in ATM$^{-/-}$ and WT teratomas (Figure 6C). Once the conditions for differentiating hESCs into Purkinje neurons are established, the ATM$^{-/-}$ hESCs will be used to further investigate the roles of ATM in the development and maintenance of the Purkinje neurons.

Cells derived from A-T patients undergo accelerated telomere shortening (Shiloh, 1995). Therefore, we examined the telomere length in cells differentiated from WT and ATM$^{-/-}$ hESCs. Since teratoma generated from hESCs provides a comprehensive mixture of differentiated cells, we determined the average telomere length in the genomic DNA derived from teratomas generated by WT and ATM$^{-/-}$ hESCs. Our findings indicate that the average telomere length in WT teratomas is 20%–30% longer than that in ATM$^{-/-}$ teratomas, indicating the potential to employ ATM$^{-/-}$ hESCs to further study the roles of ATM in telomere maintenance (Figures 6D and 6E). In summary, these findings demonstrate the feasibility to employ genetically modified hESCs and their capability to form teratomas in SCID mice for in vivo modeling of human diseases.

p53-Dependent Function Is Abolished in p53$^{-/-}$ hESCs

When injected into SCID mice, p53$^{-/-}$ hESCs gave rise to teratomas containing cells derived from each of the three germ layers, indicating that these cells remained pluripotent (Figure S4). The generation of p53$^{-/-}$ hESCs provides us the unique opportunity to study the roles of p53 in DNA-damage responses and genetic stability in hESCs. Compared with that in p53$^{+/+}$ hESCs, p53-dependent induction of p21 and Noxa mRNAs, as well as Mdm2, was abolished in p53$^{-/-}$ hESCs after DNA damage (Figures 7A and 2G). In addition, when compared with those in WT hESCs, the basal levels of p21 expression in the absence of DNA damage were also greatly reduced in p53$^{-/-}$ hESCs (Figure 7A). Together, these data indicate that p53 is transcriptionally active in hESCs and is greatly induced in hESCs after DNA damage.

Nanog, a homeodomain protein required for the self-renewal of ESCs, is an important coordinator of DNA-damage response and self-renewal in ESCs (Xu, 2005). In this context, the expression of Nanog is suppressed directly by p53 in mouse ESCs after DNA damage (Lin et al., 2005). Nanog expression is also reduced in WT hESCs rapidly after DNA damage in a p53-dependent manner, indicating an evolutionarily conserved role of p53 in coordinating DNA-damage response and self-renewal in ESCs (Figure 7B).

As an apparent difference between mouse and human cells, p53 is required for the G_2/M checkpoint in human cells after DNA damage but dispensable for G_2/M checkpoint in mouse cells (Sancar et al., 2004; Song et al., 2007). Therefore, we investigated whether p53 is required for the G_2/M checkpoint in hESCs. Control WT hESCs undergo robust G_2/M arrest after IR, and this checkpoint is impaired in p53$^{-/-}$ hESCs, indicating that p53 plays a role in cell-cycle G_2/M checkpoint in hESCs after DNA damage (Figure 7C).

While ATM$^{-/-}$ hESCs appear to be genetically stable, similarly to p53$^{-/-}$ somatic cells, chromosomal aneuploidy was observed in a small fraction (10%–20%) of the p53$^{-/-}$ hESCs (Figure S2C). In this context, the deletion of the long arm of chromosome 9 was observed in two of the twenty metaphases of each of the two independently generated p53$^{-/-}$ hESCs examined. In addition, two metaphases exhibited the duplication of chromosome 17 and 20, respectively. Therefore, the increased spontaneous genomic instability in p53$^{-/-}$ hESCs suggests that p53 plays an important role in maintaining genetic stability in hESCs.

DISCUSSION

hESCs can undergo unlimited self-renewal and be differentiated into all cell types in the body. Therefore, efficient genetic manipulation technology of hESCs will revolutionize our approach to study the cellular and developmental functions of human genes. By resolving the technical bottleneck to allow efficient gene targeting through homologous recombination in hESCs, the BAC-based gene targeting strategy will greatly facilitate the research to genetically modify hESCs into human disease

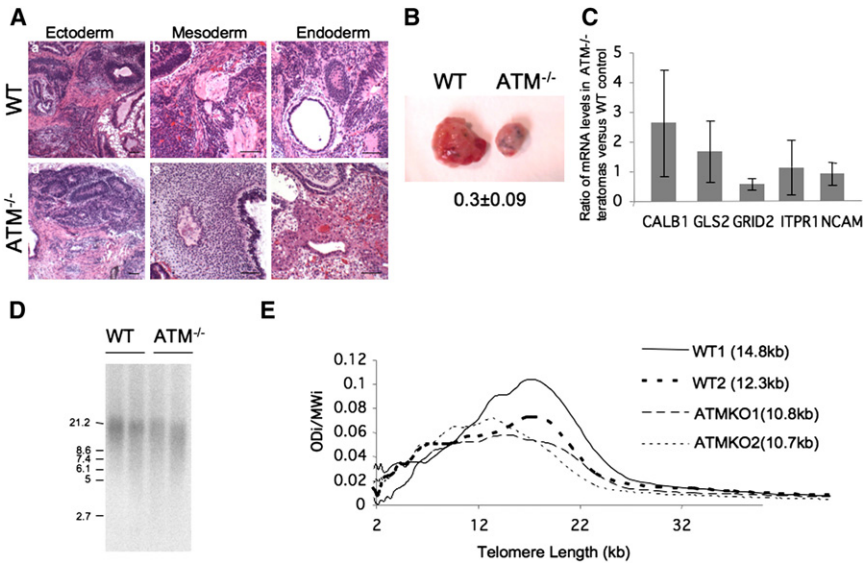

Figure 6. Teratomas Formation by ATM$^{-/-}$ hESCs in SCID Mice

(A) Teratomas formed by WT and ATM$^{-/-}$ hESCs both contain the cell types derived from each of the three embryonic germ layers. For example, neural Rosette, adipocytes, and smooth muscle (Aa); Skeletal muscle (Ab); gut and smooth muscle (Ac); neural rosette and smooth muscle (Ad); bone (Ae); and liver (Af).

(B) Representative image of teratomas formed by the same number of ATM$^{-/-}$ hESCs and WT hESCs implanted in the same SCID mice. The mean ratio of the weight of the three sets of ATM$^{-/-}$ tumor versus WT tumor is presented with standard derivation.

(C) The ratio of mRNA levels of neural cell adhesion molecule 1 (NCAM1); glutaminase (GLS2); calbindin 1 (CALB1); inositol 1,4,5-triphosphate receptor, type 1 (ITPR1); and glutamate receptor, ionotropic, delta 2 (GRID2) genes in ATM$^{-/-}$ teratomas versus WT tumor. The mRNA levels of each gene were determined by real-time PCR and standardized by the mRNA levels of GAPDH. Mean ratio from three sets of ATM$^{-/-}$ and WT tumors are shown with standard derivation.

(D) Southern blotting analysis of telomere length in the genomic DNA of four teratomas, two generated with WT hESCs and two by ATM$^{-/-}$ hESCs. Genomic DNA derived from teratomas was digested with HinfI and RsaI, and hybridized with telomere-specific digoxigenin (DIG)-labeled probe, which was detected by anti-DIG-alkaline phosphatase and chemiluminescence. Molecular weight markers are indicated on the left.

(E) The average telomere length in ATM$^{-/-}$ teratomas is shorter than that in WT teratomas. Mean telomere length was calculated from $\sum$ODi/($\sum$ODi/$\sum$MWi). ODi and MWi are optical density and molecular weight at a given position i, respectively. The average telomere length of each teratomas is indicated next to the genotype. See also Figure S3.

models for mechanistic studies and drug discovery. When compared with the gene targeting strategy with the standard targeting vector, the BAC based strategy has some obvious advantages. First, while the standard targeting vector needs to be generated with genomic DNA isogenic to the hESCs to allow higher frequency of homologous recombination, the BAC-based targeting vector derived from commercial sources can achieve high efficiency of homologous recombination in hESCs of various genetic backgrounds. In addition, while the generation of the standard targeting vectors involves complex and sometimes technically difficult cloning strategies, the recombineering technology in bacteria allows rapid genetic modification of the BAC sequence. These advantages will enable timely generation of BAC-targeting vectors for high efficiency gene targeting in hESCs. However, considering the large size of the homologous arms in the BAC targeting vector, one drawback for the BAC-based targeting approach is the difficulty to confirm the homologous recombination event. This problem is partially mitigated by our strategy to shorten one of the homologous arms with recombineering to allow the confirmation of the proper targeting with Southern blotting.

Recent advances of using zinc-finger nuclease (ZFN)-mediated genome editing has also enabled high efficiency of genetic manipulation in hESCs (Hockemeyer et al., 2009; Zou et al., 2009). When compared with the ZFN-mediated strategy, the BAC-based strategy might offer two potential advantages. First, the success of the ZFN-mediated strategy depends on the design of zinc finger motifs that can specifically bind to the endogenous genomic sequences around the targeting loci. This could be a time-consuming task since the designed zinc finger needs to be experimentally optimized for the high binding specificity for the target sequence. In this context, the DNA-binding specificity of the designed zinc finger proteins in cells remains to be validated with vigorous genomic analysis, such as ChIP-Seq technology. Therefore, to avoid the binding of designed zinc finger proteins to the unexpected locations in the genome would be a technical bottleneck for the ZFN-mediated strategy. This ''off-target'' effect of the designed ZFN would be even more problematic when the targeted genes are involved in maintaining genomic stability in hESCs, because multiple double-strand breaks introduced by ZFN in the genome will promote chromosomal translations, especially when the DNA damage response pathways are disrupted (Shiloh, 2003).

Recent groundbreaking discovery that somatic cells can be reprogrammed into the induced pluripotent stem cells (iPSCs) with defined factors has provided tremendous potential for developing human disease models (Dimos et al., 2008; Ebert et al., 2009; Takahashi and Yamanaka, 2006). While iPSCs provide a unique opportunity to model human diseases with unknown or complex genetic traits, iPSC technology might not be suitable to develop disease models for human genetic instability syndromes, such as the ones reported here, because the adult somatic cells derived from such patients will have already harbored cell-specific genetic alterations, preventing their use as generic disease models. In addition, based on the findings that the reprogramming factors mostly have oncogenic potential and that tumor suppression pathways appear to inhibit the reprogramming (Krizhanovsky and Lowe, 2009; Deng and Xu, 2009), the genetic stability and tumorigenic potential of iPSCs needs to be vigorously investigated before their potential in drug discovery can be fully realized.

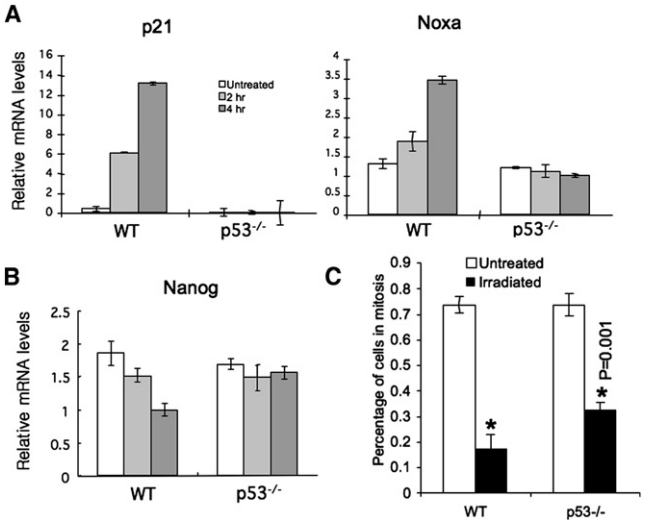

Figure 7. p53-Dependent Functions Are Abolished in p53$^{-/-}$ hESCs

(A) p53-dependent expression of p21 and Noxa mRNA is abolished in p53$^{-/-}$ hESCs after DNA damage induced by Doxorubicin. The mRNA levels of each gene were determined by real-time PCR and standardized by the mRNA levels of GAPDH.

(B) p53-dependent suppression of Nanog expression is abolished in p53$^{-/-}$ hESCs after DNA damage. Mean values from three independent experiments are shown with standard derivation.

(C) G_2/M checkpoint is impaired in p53$^{-/-}$ hESCs after IR. Mean values from three independent experiments are shown with standard derivation. p value between the irradiated WT and p53$^{-/-}$ hESCs is shown. Consistent data were obtained from two independent p53$^{-/-}$ hESCs. See also Figure S4.

Considering the critical roles of ATM and p53 in maintaining genetic stability and tumor suppression (Xu, 2006), the ATM$^{-/-}$ and p53$^{-/-}$ hESCs we established will become valuable resources to study human tumorigenesis and develop more effective therapeutic interventions for human cancer. Our studies of the ATM$^{-/-}$ hESCs indicate that, despite their defects in DNA repair and cell-cycle checkpoint, ATM$^{-/-}$ hESCs remain genetically stable. Since ATM$^{-/-}$ human somatic cells exhibit extensive genomic instability (Shiloh, 2003), this finding further highlights the existence of distinct mechanisms involved in maintaining genomic stability in hESCs and somatic cells. In addition, while our data suggest that p53 is important in maintaining genomic stability in both hESCs and somatic cells, the functions of p53 in hESCs might be different from those in somatic cells. In this context, some of the well-established p53 functions in somatic cells, such as cell-cycle G_1/S checkpoint, cellular senescence, and apoptosis, do not operate efficiently in ESCs (Xu, 2005). Therefore, similarly to that in mouse ESCs (Lin et al., 2005), one important role of p53 in maintaining genomic stability in hESCs could be to suppress Nanog expression after DNA damage, leading to the differentiation of DNA damaged hESCs and, thus, maintaining the genomic stability in the self-renewing hESCs.

EXPERIMENTAL PROCEDURES

Construction of BAC-Based Targeting Vectors

The BAC clones were from the RPCI-11 Human Male BAC Library (Osoegawa et al., 2001) and purchased from Invitrogen. The BAC based targeting vector was generated with recombineering (Copeland et al., 2001). *E. coli* strain SW106 was transformed with BAC DNA spanning human ATM, p53, or HPRT locus (Warming et al., 2005). To allow the efficient expression of the selection markers in hESCs, the PGK promoter of the selection markers was replaced with CMV early enhancer/chicken β actin (CAG) promoter that is highly active in hESCs. For the secondary targeting in hESCs, the IRES-Puro DNA fragment was inserted between the Neo and PolyA signal so that Neo and Puro are expressed simultaneously. About one kb homologous arms were inserted on the 5′ and 3′ of the selection cassettes, which was transfected into the SW106 harboring the ATM or p53 BAC to allow the insertion of the selection cassette into the BAC through homologous recombination. To shorten one homologous arm of the BAC targeting vector, AmpR genes flanked by 0.5 kb of target sequence from the homologous arm and 0.5 kb of a sequence from the backbone were introduced into the recombineering bacterial harboring the BAC-targeting vector. Homologous recombination will replace the genomic DNA of the BAC between the target sequence and backbone with AmpR gene and, thus, confer resistance to ampicillin to the bacteria.

Culture and Treatment of hESCs

The HUES cells were cultured on feeder layer in knockout DMEM supplemented with 10% knockout serum replacement (KSR), 10% plasmanate, PenStrep, Glutamine, nonessential amino acids, 10 ng/ml bFGF, and 55 μM β-mecaptoethanol, as described (Cowan et al., 2004). To culture the hESCs in the absence of feeder layer, the hESCs were cultured on matrigel-treated plates in the TESR medium supplemented with MEF conditional medium. All tissue culture reagents are purchased from Invitrogen. For passaging hESCs, confluent culture was washed with PBS, trypsinized for 5 min, resuspended in culture medium into single cell, and plated at 1:5 to 1:8 ratios.

For the electrophoration of BAC vectors into hESCs, 20 million hESCs were washed twice with PBS and mixed with 100 μg of DNA for 5 min on ice. Electroporation was conducted with a Biorad Gene Pulser II (320 V, 200 μF). The transfected cells were plated on feeder layer and, 2 days later, selected with G418 (50 μg/ml) or Puromycin (0.5 μg/ml). Surviving colonies were individually picked and expanded.

H9 cells were maintained as previously described (Thomson et al., 1998). Two hours before dissociating with Accutase (Millipore), H9 cells were treated with 10 μM ROCK inhibitor Y-27632 (Calbiochem). After electroporation with the BAC targeting vector, transfected cells were incubated with 10 μM Y-27632 for 24 hr.

All human ESC work has been approved by UCSD ESCRO and IRB.

Karyotyping and SNP-CGH Analysis

Karyotyping of the mutant hESC clones was carried out by Cell Line Genetics (Madison, WI). SNP-CGH analysis was carried out by Expression Analysis, Inc. (Durham, NC).

Taqman PCR Assay to Detect ATM Gene Copy Number

Real-time PCR reaction was carried out with 5 ng of genomic DNA, 250 nM of Taqman probes, and 500 nM of primers. Sequences of primers are as follows: GAPDHF, 5′-CCC CAC ACA CAT GCA CTT ACC-3′; GAPDHR, 5′-CCT AGT CCC AGG GCT TTG ATT-3′; GAPDH probe, 5′-(HEX) AAA GAG CTA GGA AGG ACA GGC AAC TTG GC (IOWA BLACK FQ)-3′, ATMF, 5′- TCA TCA GCT TTG CAG GCA TTA T-3′;ATMR, 5′-TGC AAA TGC TGG AAC AAC ATG-3′; and ATM probe, 5′-(FAM) TAA TTG TTG CAC CCA TTC TCC AA (IOWA BLACK FQ)-3′.

Radiosensitivity Assay of hESCs

hESCs were plated on feeder layer in 12-well plate with a density of 2000 cells/well. One day after plating, the cells were mock-treated or treated with increasing dosages of IR. After 2 weeks, the surviving colonies were stained with crystal violet and counted.

Teratoma Formation in SCID Mice

Two to three million hESCs were suspended in the knockout medium supplemented with 30% matrigel (BD Biosciences) and injected subcutaneously into SCID mice. Teratomas were recovered 6 weeks after implantation, fixed in 10% buffered formalin, embedded in paraffin, and sectioned. All sections

were stained with hematoxylin and eosin for histological assessment as previously described (Chao et al., 2006). All animal work has been approved by UCSD IACUC.

EB Formation and EB-Mediated Differentiation into Human Fibroblast

Subconfluent hESCs were washed with PBS, treated with 1 mg/ml collagenase type IV for 10 min at 37°C, and harvested with a cell scraper. After the dissociation with pipetting, cells were grown on a low-binding plate in medium consisting of KO-DMEM, 20% knockout serum replacement (KSR), nonessential amino acids, glutamine, penicillin/streptomycin, and 0.55 μM β-mercaptoethanol. Since embryoid bodies (EBs) are growing in suspension, half of the medium was changed every other day.

To derive fibroblasts from hESCs, the EBs with 7 days of suspension culture were seeded onto gelatin-coated tissue culture plates in differentiation medium consisted of DMEM supplemented with glutamine and 10% (v/v) fetal calf serum (FCS). Four to five days after initial seeding of the EBs, a confluent monolayer was trypsinized and passaged on gelatin-coated plates.

Western Blotting Analysis

Protein extracts were resolved on 6%–10% SDS-PAGE gels and transferred to nitrocellulose membrane, which was probed with a monoclonal antibody against p53 (pAb1801; Santa Cruz Biotechnology, Santa Cruz, CA) or polyclonal antibody against β-actin (Santa Cruz Biotechnology) or monoclonal antibody against ATM (Rockland, Gilbertsville, PA). Phosphorspecific antibodies were purchased from Cell Signaling Technology (Danvers, MA). The membrane was subsequently probed with a horseradish peroxidase-conjugated secondary antibody and developed with ECL PLUS (Amersham, Piscataway, NJ).

Cell-Cycle Analysis

Cell cycle G_2/M checkpoint was analyzed as previously described (Song et al., 2007). Asynchronously growing hESCs were irradiated with various dosages of IR and harvested 1 hr after IR. Cells in mitosis were identified by staining with propidium iodide for DNA content and an FITC-conjugated antibody recognizing histone H3 phosphorylated at Ser 10 (Upstate, Charlottsville, VA).

Quantitative Real-Time PCR

Total RNA from hESCs or fibroblasts was isolated using Trizol (Invitrogen, Carlsbad, CA) and RNAeasy Mini Kit (QIAGEN, Valencia, CA). One microgram of total RNA was reverse-transcribed using Superscript II RT (Invitrogen). Real-time PCR was performed with an ABI Prism 7000 (Applied Biosystems, Foster City, CA) with Power SyberGreen PCR Master Mix (Applied Biosystems, Foster City, CA). The PCR conditions were as follows: 10 min at 95°C, 40 cycles of 15 s at 95°C, and 1 min at 60°C. The average Ct value for each gene was determined from triplicate reactions and normalized with the levels of GAPDH as previously described (Song et al., 2007). The sequence of the primers are as follows: Calb1 5′ACAGTGGCTTCATAGAAACTGAG3′, 5′CCACACATTTTG ATTCCCTGGA3′; GLS2 5′TCTTCCGAAAGTGTGTGAGCA3′, 5′GACATCCTC AAAGATGCGATCC3′; GRID2 5′CTCTTGGTTTTGTCCGTCTGG3′, 5′GCAGT GCGAAATACCTCATCATC3′; ITPR1 5′TCCAGCATGACCCATGTCG3′, 5′CAC TGAGGGCTGAAACTCCAG3′; NCAM1 5′TCTATAACGCCAACATCGACGA3′, 5′TTGGCGCATTCTTGAACATG3′.

Immunoflourescence Microscopy

Human fibroblasts grown on coverslip were exposed to 2 Gy γ-irradiation and 30 min later fixed with methanol:acetone (50:50) for 10 min at −20°C. The fixed cells were blocked with 3% BSA in PBS and incubated with mouse monoclonal antibody specific for phosphorylated ATM at 1981 (1:600 dilution) or a rabbit polyclonal phosphor-specific antibody against H2AX-139p (1:200) in 1% BSA in PBS overnight at 4°C. After washing, the cells were incubated with secondary antibodies for 1 hr at room temperature. After mounting on glass slides with VECTASHIELD mounting media with DAPI (Vector Laboratories, Burlingame, CA), images were acquired by Olympus confocal microscope.

TRF Assay

TRF (Terminal Restriction Fragments) assay was performed using Telo TAGGG Telomere Length Assay as instructed by the manufacturer (Roche, NJ). Chemiluminscent signal was scanned by Typhoon Trio and analyzed by Imagequant TL software (GE Healthcare). Mean TRF length was calculated from $\sum$ODi/($\sum$ODi/$\sum$MWi). ODi and MWi are optical density and molecular weight at a given position i, respectively.

SUPPLEMENTAL INFORMATION

Supplemental Information includes four figures and can be found with this article online at doi:10.1016/j.stem.2009.11.016.

ACKNOWLEDGMENTS

We thank Dr. Melton's lab and Harvard University for providing the HUES cell lines and Drs. T. Zhao and J.-Y. Jung for technical help. This work was supported by a grant from California Institute of Regenerative Medicine to Y.X. (RC1-148).

Received: June 30, 2009
Revised: September 20, 2009
Accepted: November 25, 2009
Published: January 7, 2010

REFERENCES

Barlow, C., Hirotsune, S., Paylor, R., Liyanage, M., Eckhaus, M., Collins, F., Shiloh, Y., Crawley, J.N., Ried, T., Tagle, D., and Wynshaw-Boris, A. (1996). Atm-deficient mice: a paradigm of ataxia telangiectasia. Cell *86*, 159–171.

Chao, C., Herr, D., Chun, J., and Xu, Y. (2006). Ser18 and 23 phosphorylation is required for p53-dependent apoptosis and tumor suppression. EMBO J. *25*, 2615–2622.

Copeland, N.G., Jenkins, N.A., and Court, D.L. (2001). Recombineering: a powerful new tool for mouse functional genomics. Nat. Rev. Genet. *2*, 769–779.

Costa, M., Dottori, M., Sourris, K., Jamshidi, P., Hatzistavrou, T., Davis, R., Azzola, L., Jackson, S., Lim, S.M., Pera, M., et al. (2007). A method for genetic modification of human embryonic stem cells using electroporation. Nat. Protoc. *2*, 792–796.

Cowan, C.A., Klimanskaya, I., McMahon, J., Atienza, J., Witmyer, J., Zucker, J.P., Wang, S., Morton, C.C., McMahon, A.P., Powers, D., and Melton, D.A. (2004). Derivation of embryonic stem-cell lines from human blastocysts. N. Engl. J. Med. *350*, 1353–1356.

Davis, R.P., Ng, E.S., Costa, M., Mossman, A.K., Sourris, K., Elefanty, A.G., and Stanley, E.G. (2008). Targeting a GFP reporter gene to the MIXL1 locus of human embryonic stem cells identifies human primitive streak-like cells and enables isolation of primitive hematopoietic precursors. Blood *111*, 1876–1884.

Deng, W., and Xu, Y. (2009). Genome integrity: linking pluripotency and tumorgenicity. Trends Genet. *25*, 425–427.

Dimos, J.T., Rodolfa, K.T., Niakan, K.K., Weisenthal, L.M., Mitsumoto, H., Chung, W., Croft, G.F., Saphier, G., Leibel, R., Goland, R., et al. (2008). Induced pluripotent stem cells generated from patients with ALS can be differentiated into motor neurons. Science *321*, 1218–1221.

Donehower, L.A., Harvey, M., Slagle, B.L., McArthur, M.J., Montgomery, C.A., Jr., Butel, J.S., and Bradley, A. (1992). Mice deficient for p53 are developmentally normal but susceptible to spontaneous tumours. Nature *356*, 215–221.

Ebert, A.D., Yu, J., Rose, F.F., Jr., Mattis, V.B., Lorson, C.L., Thomson, J.A., and Svendsen, C.N. (2009). Induced pluripotent stem cells from a spinal muscular atrophy patient. Nature *457*, 277–280.

Elson, A., Wang, Y., Daugherty, C.J., Morton, C.C., Zhou, F., Campos-Torres, J., and Leder, P. (1996). Pleiotropic defects in ataxia-telangiectasia protein-deficient mice. Proc. Natl. Acad. Sci. USA *93*, 13084–13089.

Hockemeyer, D., Soldner, F., Beard, C., Gao, Q., Mitalipova, M., DeKelver, R.C., Katibah, G.E., Amora, R., Boydston, E.A., Zeitler, B., et al. (2009). Efficient targeting of expressed and silent genes in human ESCs and iPSCs using zinc-finger nucleases. Nat. Biotechnol. *27*, 851–857.

Irion, S., Luche, H., Gadue, P., Fehling, H.J., Kennedy, M., and Keller, G. (2007). Identification and targeting of the ROSA26 locus in human embryonic stem cells. Nat. Biotechnol. *25*, 1477–1482.

Jacks, T., Remington, L., Williams, B.O., Schmitt, E.M., Halachmi, S., Bronson, R.T., and Weinberg, R.A. (1994). Tumor spectrum analysis in p53-mutant mice. Curr. Biol. *4*, 1–7.

Johnson, B.V., Shindo, N., Rathjen, P.D., Rathjen, J., and Keough, R.A. (2008). Understanding pluripotency—how embryonic stem cells keep their options open. Mol. Hum. Reprod. *14*, 513–520.

Ko, L.J., and Prives, C. (1996). p53: puzzle and paradigm. Genes Dev. *10*, 1054–1072.

Krizhanovsky, V., and Lowe, S.W. (2009). Stem cells: The promises and perils of p53. Nature *460*, 1085–1086.

Lara-Tejero, M., and Galán, J.E. (2000). A bacterial toxin that controls cell cycle progression as a deoxyribonuclease I-like protein. Science *290*, 354–357.

Lin, T., Chao, C., Saito, S., Mazur, S.J., Murphy, M.E., Appella, E., and Xu, Y. (2005). p53 induces differentiation of mouse embryonic stem cells by suppressing Nanog expression. Nat. Cell Biol. *7*, 165–171.

Mills, A.A. (2005). p53: link to the past, bridge to the future. Genes Dev. *19*, 2091–2099.

Osoegawa, K., Mammoser, A.G., Wu, C., Frengen, E., Zeng, C., Catanese, J.J., and de Jong, P.J. (2001). A bacterial artificial chromosome library for sequencing the complete human genome. Genome Res. *11*, 483–496.

Ruby, K.M., and Zheng, B. (2009). Gene targeting in a HUES line of human embryonic stem cells via electroporation. Stem Cells *27*, 1496–1506.

Sancar, A., Lindsey-Boltz, L.A., Unsal-Kaçmaz, K., and Linn, S. (2004). Molecular mechanisms of mammalian DNA repair and the DNA damage checkpoints. Annu. Rev. Biochem. *73*, 39–85.

Shiloh, Y. (1995). Ataxia-telangiectasia: closer to unraveling the mystery. Eur. J. Hum. Genet. *3*, 116–138.

Shiloh, Y. (2003). ATM and related protein kinases: safeguarding genome integrity. Nat. Rev. Cancer *3*, 155–168.

Shiloh, Y., and Kastan, M.B. (2001). ATM: genome stability, neuronal development, and cancer cross paths. Adv. Cancer Res. *83*, 209–254.

Song, H., Hollstein, M., and Xu, Y. (2007). p53 gain-of-function cancer mutants induce genetic instability by inactivating ATM. Nat. Cell Biol. *9*, 573–580.

Takahashi, K., and Yamanaka, S. (2006). Induction of pluripotent stem cells from mouse embryonic and adult fibroblast cultures by defined factors. Cell *126*, 663–676.

Thomson, J.A., Itskovitz-Eldor, J., Shapiro, S.S., Waknitz, M.A., Swiergiel, J.J., Marshall, V.S., and Jones, J.M. (1998). Embryonic stem cell lines derived from human blastocysts. Science *282*, 1145–1147.

Urbach, A., Schuldiner, M., and Benvenisty, N. (2004). Modeling for Lesch-Nyhan disease by gene targeting in human embryonic stem cells. Stem Cells *22*, 635–641.

Warming, S., Costantino, N., Court, D.L., Jenkins, N.A., and Copeland, N.G. (2005). Simple and highly efficient BAC recombineering using galK selection. Nucleic Acids Res. *33*, e36.

Watanabe, K., Ueno, M., Kamiya, D., Nishiyama, A., Matsumura, M., Wataya, T., Takahashi, J.B., Nishikawa, S., Nishikawa, S.-i., Muguruma, K., and Sasai, Y. (2007). A ROCK inhibitor permits survival of dissociated human embryonic stem cells. Nat. Biotechnol. *25*, 681–686.

Xu, Y. (2005). A new role for p53 in maintaining genetic stability in embryonic stem cells. Cell Cycle *4*, 363–364.

Xu, Y. (2006). DNA damage: a trigger of innate immunity but a requirement for adaptive immune homeostasis. Nat. Rev. Immunol. *6*, 261–270.

Xu, Y., and Baltimore, D. (1996). Dual roles of ATM in the cellular response to radiation and in cell growth control. Genes Dev. *10*, 2401–2410.

Xu, Y., Ashley, T., Brainerd, E.E., Bronson, R.T., Meyn, M.S., and Baltimore, D. (1996). Targeted disruption of ATM leads to growth retardation, chromosomal fragmentation during meiosis, immune defects, and thymic lymphoma. Genes Dev. *10*, 2411–2422.

Xue, H., Wu, S., Papadeas, S.T., Spusta, S., Swistowska, A.M., MacArthur, C.C., Mattson, M.P., Maragakis, N.J., Capecchi, M.R., Rao, M.S., et al. (2009). A targeted neuroglial reporter line generated by homologous recombination in human embryonic stem cells. Stem Cells *27*, 1836–1846.

Zou, J., Maeder, M.L., Mali, P., Pruett-Miller, S.M., Thibodeau-Beganny, S., Chou, B.-K., Chen, G., Ye, Z., Park, I.-H., Daley, G.Q., et al. (2009). Gene targeting of a disease-related gene in human induced pluripotent stem and embryonic stem cells. Cell Stem Cell *5*, 97–110.

Zwaka, T.P., and Thomson, J.A. (2003). Homologous recombination in human embryonic stem cells. Nat. Biotechnol. *21*, 319–321.